

Eddy modulation of air-sea interaction and convection

IVANA CEROVEČKI, JOHN MARSHALL

54-1726 Dept. of Earth, Atmospheric, and Planetary Sciences
Massachusetts Institute of Technology, Cambridge, MA 02139-4307

July 5, 2006

E-mail: ivana@rossby.mit.edu; jmarsh@mit.edu

Abstract

Eddy modulation of the air-sea interaction and convection that occurs in the process of mode water formation is analyzed in simulations of a baroclinically unstable wind- and buoyancy-driven jet. The water mass transformation analysis of Walin (1982) is used to estimate the formation rate of mode water and to characterize the role of eddies in that process.

It is found that diabatic eddy heat flux divergences in the mixed layer are comparable in magnitude, but of opposite sign, to the surface air-sea heat flux, and largely cancel the direct effect of buoyancy loss to the atmosphere. Our calculations suggest that mode water formation estimates based on climatological air-sea heat flux data and outcrops which do not fully resolve ocean eddies, may neglect a large opposing term in the heat budget and are thus likely to significantly over-estimate true formation rates. In Walin's water mass transformation framework, this manifests itself by a sensitivity of formation rates estimates to the averaging period over which the outcrops and air-sea fluxes are subjected.

The key processes are described in terms of a transformed Eulerian-mean formalism in which eddy-induced mean flow tends to cancel the Eulerian-mean flow, resulting in weaker residual mean flow, subduction and mode water formation rates.

1 Introduction

A census of the volume of water in different temperature classes in the thermocline of the north Atlantic Ocean shows a peak at 18°C; hence its characterization as a “mode water”. Eighteen degree water (EDW) is thought to be formed in wintertime convection in the western North Atlantic just south of the Gulf Stream, in the presence of strong shear with competing effects of vertical and lateral mixing, advection and stirring working together to set its properties (e.g. Worthington 1959, 1976; Schroeder et al, 1959; Ebbesmeyer and Lindstrom, 1986). A characteristic feature of EDW is its low potential vorticity which tags the water mass and allows it to be mapped far from its source (see McCartney, 1982). Although EDW is a historically well-observed property of the subtropical gyre but the relative importance of the different processes that produce this major feature is still debated. Numerical models can capture mode water formation (e.g. Hazeleger and Drijfhout, 1998, 1999, 2000; Marsh and New, 1996; Paiva and Chassignet, 2002). However, there is a considerable disconnect between various estimates of EDW formation: whereas up to 15-20 Sv of formation are implied by climatological air-sea flux measurements using Walin’s (1982) framework (Speer and Tziperman, 1992), only 5 Sv have been estimated to be injected seasonally into the subtropical gyre, both from observations using profiling floats (Kwon and Riser, 2005 a,b) and inferences based on thermocline diapycnal mixing rates. The discrepancy clearly indicates that the relative importance of the various processes contributing to mode water formation and dissipation rates is not yet well understood. However, closing the budget is an important matter since mode waters are the primary water mass that interacts with the atmosphere in key regions of air-sea interaction such as the Gulf Stream and its recirculation.

It is generally accepted that mode waters are formed in the process of winter vertical convection which is triggered by heat loss from the ocean to the atmosphere, and so can be modulated by, for example, the NAO (see Marsh and New, 1996). However, when analyzing data from the Panulirus station, Jenkins (1982) obtained a poor correlation between local surface air-sea flux and variations in the properties of subtropical mode water. Similarly,

Talley and Raymer (1982), analyzing data from the same station, observed that “in fact, the heat flux was nearly out of phase with the Eighteen Degree Water properties”. This imperfect correlation between local surface air-sea flux and variations in the properties of subtropical mode water may be an indication that there are processes other than surface heat loss that play an important role in mode water formation.

Since mode waters tend to form adjacent to strong baroclinically unstable fronts, eddy processes may play a central role in mode water formation and dispersal (see Dewar, 1986). Indeed, David Marshall (1997; DM97 hereafter) showed that mesoscale eddies provide a mechanism to modify the rate at which a water mass is transferred from the surface mixed layer of the ocean into the ocean interior, in particular in regions of strong baroclinic instability. Dong and Kelly (2004) analyzed the importance of ocean advection and heat storage for the heat budget in the Gulf Stream region using a simple three-dimensional thermodynamic model. They found some indication that variations in ocean heat content appear to induce air-sea heat fluxes over the Gulf Stream (their Figure 13). The authors suggest that advection of anomalies in boundary currents may “precondition” the water column for mode water formation. Kelly (2004) reported similar results for the western North Pacific and also found that latitudinal variations of heat content and surface flux were negatively correlated.

As an introduction to the processes under consideration in this paper, consider a frontal system with warm water on one side and cold water on the other side, as sketched in Fig.1. The isopycnals are tilted, so there is both horizontal and vertical shear and the frontal region will be baroclinically unstable, generating eddies which drive the sea-surface temperature out of equilibrium with the temperature of the atmosphere above. Since baroclinic eddies stir horizontally, they transport colder water towards the warm side of the front, water on the warmer side becomes colder than the atmosphere above it and gains heat from the atmosphere. Similarly, water on the cold side of the front becomes warmer than the atmosphere above and so loses heat to the atmosphere. Such air-sea heat exchange, if acting alone, would drive diapycnal volume fluxes giving rise to divergent volume flow across the isopyc-

nals, drawing fluid from the interior towards the surface (as sketched in Fig.1a). However, lateral eddy fluxes directed down the mean temperature gradient induce a convergent diapycnal volume flow and subduction that opposes the divergent surface flow set up by air-sea heat flux (Fig.1b). If the eddy heat flux is stronger than the air-sea heat flux, diapycnal flow will be convergent and give rise to subduction which can carry low PV fluid formed at the surface into the interior (Fig.1c). In such a case mode water properties may be in phase with the eddy heat flux but out of phase with the air-sea heat flux. Thus the volume and properties of mode water might not then be directly slaved to the air-sea flux, but also depend on the nature of lateral eddy processes. The flows sketched in Fig.1a and discussed above are required to satisfy volume and heat budgets. They may be realized dynamically in many different ways, depending on the detailed nature of the flow and the flow geometry.

In this work we analyze an idealized numerical front, as schematically shown in Fig.1, that becomes unstable and displays mode water formation. Our eddy-resolving model contains key features that are believed to be important in mode water formation: the presence of vigorous eddies adjacent to a strongly sheared baroclinic front, with the resulting formation of low PV water by convective processes triggered by strong air-sea heat exchange and modulated by mesoscale eddies. We address the relative importance of the various processes involved in mode water formation and dissipation, in particular the competing roles of air-sea heat flux and eddy heat flux. We also study the effect of eddy processes in modulating air-sea interaction and convection and hence the properties of mode waters. We apply Walin's (1982) water mass formation analysis to both eddy resolving and non-eddy-resolving "data" from the model and study the difference.

Whereas DM97 developed the formalism of the Walin analysis in an eddying ocean and pointed out the importance of eddy buoyancy fluxes to the process of water formation, here we present a detailed case study with eddy resolved numerical flow fields. DM97 notes that eddy fluxes in the mixed layer include both an advective and a diapycnal component, but neglects the diapycnal part of the eddy buoyancy flux in the mixed layer when applying the

theory to the Southern Ocean circulation. We diagnose both components of eddy buoyancy flux here and find that the diapycnal component is large in the mixed layer and that its divergence largely cancels the air-sea heat flux. Our procedure is to first perform the Walin analysis on a model data set which has sufficient resolution in space and time to capture the eddies. We then “coarse grain” the same data set before carrying out the same analysis: the difference reveals the eddy effects.

The model used is the MITgcm (Marshall et al., 1997 a,b). The simplicity of the model set-up (described in Section 2.1) allows one to diagnose the heat budget in the upper ocean and separate the individual terms into mean and eddy contributions. The equilibrium state of the flow is described in Section 2.2. The diagnostic framework of Walin’s water mass transformation analysis is briefly outlined and then applied in Section 3. Since observational data sets with the necessary spatial and temporal resolution required to represent ocean eddies are rarely available, averaging either in space or time is required to define eddy related quantities. It is then necessary to account in some way for eddy heat fluxes directed laterally through the mixed layer, as sketched in Fig.1b. As described in Section 4, we suggest a way forward guided by the formalism of the Transformed-Eulerian Mean (TEM). In Section 5, the role of the air-sea coupling strength is reviewed and the effect of modifying the coupling strength in our calculations briefly examined. Discussion and conclusions are presented in Section 6.

2 Model

2.1 Model set-up

The model used is the MITgcm (Marshall et al. 1997 a,b) configured in a pie-shaped sector of the sphere and run hydrostatically. We consider the formation of mode water in the vicinity of a strong and strongly variable jet in a zonally reentrant channel on the sphere lying between the equator and $50^{\circ}S$ ¹. The model has a horizontal resolution of $1/6^{\circ}$. The sector

¹The particular calculation described here was originally designed for studies of the southern ocean — Cerovečki et al. 2006

is 10° wide in the zonal direction with periodic boundary conditions imposed at longitudinal boundaries. The model ocean is 4 km deep and has 15 vertical levels of unequal thickness, with a free slip boundary condition at the equator and a no slip boundary condition at the polar wall. The simplicity of the geometry allows one to investigate the role played by eddies in zonal-average dynamics both in terms of the conventional Eulerian mean and the TEM. Note that with zonally periodic flow reminiscent of the Southern Ocean, our results are also (and perhaps arguably more) relevant to the formation of South Atlantic Mode Water.

A linear equation of state is assumed: $\rho = \rho_0(1 - \alpha_T T)$, where α_T is the thermal expansion coefficient and T is temperature: isotherms and isopycnals coincide. The mixed layer is represented using the “KPP” scheme of Large et al. (1994). Small scale diffusion of momentum (K^v) and temperature (K^T) are also represented: a Laplacian diffusion in the vertical direction ($K_z^v = 10^{-3} \text{ m}^2\text{s}^{-1}$ and $K_z^T = 10^{-5} \text{ m}^2\text{s}^{-1}$) and biharmonic diffusion in the horizontal direction ($K_h^v = 2 \times 10^{11} \text{ m}^4\text{s}^{-1}$ and $K_h^T = 10^{10} \text{ m}^4\text{s}^{-1}$).

The flow is forced at the surface by an idealized wind stress and air-sea heat fluxes. The heat flux \mathcal{H} (in W m^{-2}) is determined by relaxing the temperature of the uppermost model layer (of thickness d_1 – here 10m — and temperature SST) to a specified equilibrium temperature T^* (shown in Figure 2) on a timescale τ thus:

$$\mathcal{H} = \rho c_w \frac{(T^* - SST)d_1}{\tau}. \quad (1)$$

Initially we set τ to 30 days, but sensitivity of our results to this relaxation time is discussed in Section 5. Both wind stress and equilibrium temperature are functions of latitude only (Fig.2.) The wind stress is directed eastward everywhere, becomes very small within $10^\circ S$ of the Equator and reaches a maximum at $33^\circ S$: the Ekman layer induces downwelling equatorward of the maximum and Ekman upwelling on the poleward side. The meridional equilibrium temperature gradient is maximum around $20^\circ S$ and marks the latitude of the mean eastward flowing jet.

The model was integrated from a state of rest with a horizontally uniform stratification.

The flow rapidly became baroclinically unstable. We show model results after 700-800 years of integration, when time-averaged budgets are close to the steady state.

2.2 Phenomenology

A snap-shot (daily average) of zonal mean temperature after 750 years of numerical integration (Fig.3, top panel) shows widely separated isopycnals between latitudes of $10^{\circ}S$ and $15^{\circ}S$ at depths of 100m to 800m, indicating the existence of a low PV pool. The low PV pool is on the equatorward flank of the core of the eastward jet (Fig.3, bottom panel). It is well known that both barotropic and baroclinic flows on the sphere develop jets (e.g. Panetta, 1993; Rhines, 1994). The present flow exhibits a strong eastward jet centered at $20^{\circ}S$ (roughly corresponding to the maximum gradient in T^*) flanked by multiple jet structures on both sides, whose presence is clearly evident both in the zonal mean zonal velocity shown in Fig.3, as well as in the instantaneous sea-surface temperatures shown in Fig.4. Close to the equator, where the wind is weak, eddy processes are not strong, and the fluid column remains rather uniformly stratified. On the poleward flank of our region of focus, surface cooling triggers convection and vertically homogenizes the fluid column over great depth (Fig.3, top panel).

Fig.4 shows a horizontal snap-shot of sea surface temperature. The zonal extent of the channel is 10° and the domain is periodic (note that three periods are plotted to facilitate visualization of the flow). The strongest eddy activity is confined between latitudes $10^{\circ}S$ and $30^{\circ}S$ and comprises a single eddy between $10^{\circ}S$ and $15^{\circ}S$. We call this the “mode one” eddy. Poleward of it, smaller scales are evident, but they are less energetic. The dominant and strongly persistent “mode one” eddy is found just equatorward of the main eastward jet. It is likely that the zonal scale of the eddy is determined by the width of the reentrant channel — initially one observes the zonal scale expanding as energy cascades to larger scales until it become as large as the geometry permits.

Reynolds stresses give rise to strong horizontal shear around $15^{\circ}S$. In the critical layer between the eastward and westward flows, the flow wraps up the contours of absolute vorticity

so that the “mode one” eddy develops a Kelvin’s cat’s eye structure — a lens-shaped region of closed streamlines within which temperature as well as vorticity is nearly uniform. The circulation along these streamlines is counterclockwise. Fine scale structures are continuously generated and dissipated. Fig.4 shows that both warm and cold water filaments are formed, with warm filaments being advected poleward and cold filaments equatorward.

Fig.5 shows daily average synoptic maps of sea surface temperature, air-sea fluxes and mixed layer depth (obtained from the KPP parameterization) at two different times separated by 22 days. As noted above, warm water is advected poleward and wrapped around the “mode one” eddy on its poleward side, thus filling a growing region (centered $\sim 15^\circ S$) between the eddy and the jet with warm water. In this manner the equatorward flank of the eastward jet is warmed, so making this region prone to convection because the atmosphere above is colder than the surface water. Heat is thus released to the atmosphere (Fig.5b), and convection results, deepening the mixed layer within the warm water filaments (Fig.5c). The sensitivity of the eddy-induced convection to the strength of the air-sea coupling is discussed in Section 5.

Such convective events generate low PV water that will subsequently be shown to feed the low PV pool. This can be seen in Fig.6 showing a typical convective event (upper panel): patches of low PV are injected into the interior by convection occurring around $16^\circ S$. After a major convective event, low PV fluid spreads along isopycnals giving rise to a low PV pool (characterized by small values of negative PV) which lies between the $20^\circ C$ and $21^\circ C$ isotherm (bottom panel). Note that in both cases (i.e. top and bottom panel) convection occurs equatorward of the main jet, whose position is indicated by tightly spaced isotherms, placed around $y \approx 20^\circ S$ in the top panel and $y \approx 16^\circ S$ in the bottom panel. (Note that Fig.6 is not zonally averaged).

To more directly document the history of fluid parcels we modeled the evolution of passive tracers in the flow. Fig.7 shows the distribution of a passive scalar for five different injections over 30 years; for each tracer the concentration in the uppermost layer is relaxed to

a specified distribution that is sharply peaked in latitude and independent of longitude with a relaxation time of three days. Appreciable concentrations are subsequently found below the surface layer only for tracers injected at the latitude corresponding to major convective events (as in release three where the concentration is peaked at $16^\circ S$ latitude). In this case the tracer is mixed down by convective events and thereafter is spread in to the ocean interior by eddy processes. The tracer ultimately fills the region of low PV.

We now go on to quantify the formation of mode water in our model and diagnose the processes responsible for it.

3 Diagnostic framework: the “Walin” formalism

3.1 Background theory

In this section we make use of Walin’s (1982) theory of water mass transformation to estimate formation rates of low PV water in our numerical simulation. Consider, in the spirit of Walin (1982), and using the notation of Garrett et al. (1995) and Marshall et al. (1999), the conservation of volume V and density (anomaly) σ for the region $R(\sigma, t)$, sketched in Fig.8, which extends laterally over the whole ocean basin and terminates at coastal boundaries; it is bounded above by the sea surface, below by a fixed interior Eulerian surface $z = -h(x, y)$, across which we wish to compute the volume flow, and laterally by surfaces of constant density, σ and σ_1 . The two isopycnal surfaces that bound the region $R(\sigma, t)$ have areas $\mathcal{A}_\sigma(\sigma, t)$ and $\mathcal{A}_\sigma(\sigma_1, t)$ (see Fig.2 in Marshall et al. (1999) and Fig.8). Here σ_1 is a conveniently chosen reference density taken to be less than σ .

Conservation of the volume V of region $R(\sigma, t)$ can be expressed as:

$$\frac{\partial V}{\partial t} = A(\sigma_1, t) - A(\sigma, t) - M(\sigma, t) \quad (2)$$

where $A(\sigma_1, t)$ is the net volume flux through the isopycnal surface labeled σ_1 (in $m^3 s^{-1}$) and M is the net volume flux across the surface $h(x, y)$ in the density interval from σ_1 to σ , integrated across the ocean basin from one coast to the other. Here A is positive for flow

that is directed from lighter to heavier fluid (i.e. poleward) and is defined by:

$$A(\sigma, t) = \int \int_{\mathcal{A}_\sigma(\sigma, t)} (\mathbf{u} - \mathbf{u}_\sigma) \cdot \hat{\mathbf{n}}_\sigma d\mathcal{A}, \quad (3)$$

where \mathbf{u}_σ is the velocity of an isopycnal surface normal to itself, which is given by

$$\mathbf{u}_\sigma = -\hat{\mathbf{n}}_\sigma \frac{\partial \sigma / \partial t}{|\nabla \sigma|}, \quad (4)$$

and $\hat{\mathbf{n}}_\sigma \equiv \nabla \sigma / |\nabla \sigma|$ is a unit vector normal to the isopycnal surface pointing in the direction of maximum density increase.

By using the conservation of density (proportional to buoyancy) written in the form:

$$\frac{\partial \sigma}{\partial t} + \nabla \cdot (\mathbf{u}\sigma + \mathbf{N}_\sigma) = 0 \quad (5)$$

where \mathbf{u} is the fluid velocity, $\mathbf{u}\sigma$ is the advective flux of density and \mathbf{N}_σ the non-advective flux of density, Walin (1982) showed that A can be related to the non-advective supply of density to the volume $R(\sigma, t)$ thus:

$$A(\sigma, t) = \frac{\partial B(\sigma, t)}{\partial \sigma}, \quad (6)$$

where

$$B = - \int \int \int_{R(\sigma, t)} \nabla \cdot \mathbf{N}_\sigma dV. \quad (7)$$

Finally, using the notation of Garrett et al. (1995) and Marshall et al. (1999), we separate B in Eqs.(6) and (7) into “surface” and “interior” contributions, to obtain:

$$A = F - \frac{\partial D}{\partial \sigma}. \quad (8)$$

Here

$$F = \frac{\partial B_S}{\partial \sigma} \quad (9)$$

is the “transformation” associated with air-sea fluxes and

$$B_S = - \int \int_{\mathcal{A}_S(\sigma,t)} \mathcal{B}_S d\mathcal{A}, \quad (10)$$

is obtained as an area integral of the air-sea density flux, \mathcal{B}_S , through the outcrop window bounded by the reference density σ_1 on one side and σ on the other side (see Fig.8). Air-sea density flux B_S is directly proportional to the air-sea heat flux (in W/m^2 , positive for ocean gaining heat). The “interior” contributions comprise the non-advective (diffusive) supply across interior density surfaces bounding the region $R(\sigma, t)$, which include two lateral isopycnal surfaces with densities σ and σ_1 and the fixed interior Eulerian surface $z = -h(x, y)$, across which we compute the volume flow:

$$D = \int \int \mathbf{N}_\sigma \cdot \hat{\mathbf{n}}_\sigma d\mathcal{A}. \quad (11)$$

The convergence of A gives the rate at which fluid is being added to (or subtracted from) a layer bounded by two adjacent isopycnals and is therefore called the “formation rate” defined by

$$\text{Formation rate} = - \frac{\partial A}{\partial \sigma}. \quad (12)$$

For more details see Marshall et al. (1999).

Note that although time does not explicitly appear, Eq.(8) is an exact expression even in the time-dependent case. Indeed, DM97 points out that the time-mean subduction of a water mass should be evaluated following the meandering surface density outcrops. Garrett and Tandon (1997) have also noted that in order to accurately estimate A using Eq.(8), it is necessary to follow the instantaneous isopycnals in time. Donners et al. (2005) recently studied water mass transformation and subduction in the South Atlantic by applying the Walin method to numerical model results obtained at eddy permitting resolution ($1/4^\circ \times 1/4^\circ$) and point out the importance of eddy processes in this calculation. The importance of following the meandering surface density outcrops is also shown very clearly in our study.

3.2 An illustration using “climatological” air-sea fluxes and outcrops

As an illustration, we first consider a Walin analysis performed using 100 annually averaged model sea-surface temperature and air-sea heat flux fields. To estimate transformation rate F due to density flux B_S in Eqs.(9) and (10), we first express the density flux in terms of air-sea heat flux using the relation:

$$\mathcal{B}_S = \frac{\alpha}{c_w} \mathcal{H} \quad (13)$$

where α is the coefficient of thermal expansion of water (taken as a positive constant in our forward integration) and c_w is the heat capacity of water. We use the heat flux \mathcal{H} (in W m^{-2}) given by Eq.(1).

The surface distribution of the air-sea heat flux \mathcal{H} is shown in the top panel of Fig.9 together with the SST averaged over 100 years. If $\mathcal{H} > 0$, then the ocean is warmed; if $\mathcal{H} < 0$ it is cooled. The zonally averaged value of this air-sea heat flux is also plotted against temperature in the top panel of Fig.10. The bottom panel of Fig.10 shows the diapycnal volume flux A obtained from Eq.(8) with neglect of interior contribution $\frac{\partial D}{\partial \sigma}$ and expressing the surface density flux using Eqs. (9), (10), (1) and (13): the diapycnal volume flux, A , implied by air-sea fluxes alone is negative (i.e. directed equatorward) equatorward of $15^\circ S$ (corresponding to the mean temperature of $\sim 21^\circ\text{C}$) and positive (poleward) poleward of this latitude. Hence, just as sketched schematically in Fig.1a, analysis of air-sea fluxes derived solely from heavily averaged surface heat flux would suggest that fluid is being drawn up towards the surface around $15^\circ S$ (in the temperature range from $\sim 21^\circ\text{C}$ to $\sim 23^\circ\text{C}$). But is this the correct sense of the diapycnal volume flux in an ocean with strong eddies? One must be cautious when working with data that have averaged out the effect of eddies. Indeed we will now show that the actual sense of the diapycnal volume flux is very different – and in fact directly opposite – when account is taken of the role of eddies. To illustrate, we will carry out a Walin analysis following instantaneous outcrops and air-sea density fluxes at

sufficiently high resolution in space and time to resolve eddies processes (Section 3.3). To estimate the significance of the role that eddies play in formation of low PV water, we go on to average these data sets over successively longer time intervals and perform a Walin analysis on increasingly “coarse-grained” data — see Fig.8 (right). How sensitive will the implied transformation rates be to the degree of “coarse-graining”?

3.3 Application of the Walin formalism to instantaneous isotherms

We first perform a Walin analysis using Eq.(8) from the output of the model simulation described in Section 2.1 that has sufficient resolution in both space and time to represent eddy processes. We use temperature data sampled each day and calculate the formation rate between the instantaneous isotherms as they move around from day to day.

The non-advective supply of density, Eq.11, is computed from N_σ taking in to account the various diffusive terms employed in the model forward run:

$$\mathbf{N}_\sigma = -\left(K_z \frac{\partial \sigma}{\partial z} \hat{\mathbf{z}} + K_H \nabla_{\mathbf{H}}[\nabla_H^2 \sigma] + K_{\gamma_\sigma} \hat{\mathbf{z}}\right) \quad (14)$$

where K_z is a vertical diffusion parameter representing both interior mixing by internal wave breaking and enhanced mixing due to convection (see Klinger et al., 1996), K_H is the coefficient of biharmonic horizontal diffusion (used to control grid-scale noise in the tracer equations) and K_{γ_σ} is the “nonlocal term” in the KPP parameterization (see Large et al., 1994).

Fig.11 shows the volume flux A (top panel) and the formation rate $\frac{\partial A}{\partial T}$ (bottom panel) both obtained using synoptic SST and air-sea heat flux data. ² We see a pronounced peak in formation of 2 Sv of water formed in the temperature class centered at 21°C. Comparison of the volume flux estimate obtained by taking both air-sea heat flux and diffusive heat flux into account in Eq.(8), with that based on only air-sea heat flux, shows that the contribution

²For consistency with the literature, especially Marshall et al. (1999), we use density as the independent variable in equations leading to the formation rate estimates. However since we use a linear equation of state with salinity assumed constant, we present the results of our calculations using temperature as the independent variable.

of the diffusive heat flux is very small relative to the air-sea heat flux (Fig.11). This is encouraging and shows that “numerical” issues, as well as resolved diffusive fluxes, do not play a significant role in setting formation rates in the model.

We see, then, that by using synoptic data we diagnose a very different pattern of A than given in Fig.10 and one that indeed implies a formation of mode water in the observed temperature range.

3.4 Walin analysis using time averaged air-sea heat flux data

In the previous section we applied the Walin analysis on synoptic data with sufficient resolution in space and time to resolve the eddies, in which case D represents the small scale diffusive heat flux. However, a data set with sufficiently fine resolution in space and time to resolve eddies is rarely available, so typically one needs to work with data that have been time-averaged at a fixed location. In order to study how averaging affects the accuracy of formation rate estimates obtained by Walin’s (1982) analysis, we time-average the temperature model results (those used in Section 3.3) on the Eulerian grid of the model and use them to calculate outcrop windows and air-sea heat fluxes. Although there is no time-dependent forcing in our model, there is intrinsic time variability due to baroclinic instability. We now compare the results of Walin’s analysis obtained using successively more heavily time-averaged data (which smooths out the temperature field and outcrop windows) with those obtained using synoptic data.

Fig.12 compares estimates of A using Eq.(8) and setting $D = 0$, but retaining the air-sea flux contribution in F via Eqs. (10), (1) and (13), using (i) daily outcrops and air-sea flux data, (ii) monthly-averaged data and (iii) yearly averaged data. As shown in the upper panel of Fig.12, the dominant process captured in all transformation rate estimates, is that the ocean loses heat in the temperature range $\sim 17^{\circ}\text{C} - 21^{\circ}\text{C}$ and gains heat in the temperature range $\sim 21^{\circ}\text{C} - 25^{\circ}\text{C}$. This pattern of air-sea heat flux is induced by the presence of the “mode one” eddy and is the only heat exchange process represented when using annually-

averaged air-sea heat flux data and outcrops. In strong contrast, use of daily air-sea heat flux data reveals a much more intense heat exchange confined to a narrow temperature range: a peak in heat loss in the temperature range $21^{\circ}\text{C} - 23^{\circ}\text{C}$ corresponding to the low PV pool. This is the typical temperature range of warm water eddy filaments (seen in Fig.4), which advect heat poleward and release it to the colder atmosphere above, triggering convection and formation of water of temperature 20.5°C to 21.5°C (Fig.12, bottom panel). This is the process responsible for mode water formation in our zonally periodic flow geometry (but for a gyre flow, like the one that includes the Gulf Stream region, mode water can also be formed even in the absence of eddies). In annually averaged data, the filaments of warm water are averaged out and so these data do not capture heat loss to the atmosphere associated with the eddy filaments and “miss” formation of mode water (there is no peak at temperatures around 21°C). As it takes tens of days for the “mode one” eddy to cross the computational domain — of some 10° of longitude — the results obtained from the monthly means are somewhat similar to those obtained using daily mean data, since monthly means still capture eddy filamentation.

The large difference in both the transformation and formation rate estimates based on synoptic (daily) and time-averaged (annually averaged) data indicates that formation rate estimates obtained from smooth climatological data, which do not resolve the eddy processes that generally oppose air-sea heat transfer processes, are likely to be in error. It is therefore of the crucial importance to work with synoptic temperature data. This is in accord with DM97, who shows that when evaluating the time-mean subduction rates, one needs to work in a Lagrangian frame of reference which follows the meandering surface density outcrops and to take into account the area over which the water mass is outcropped, and with Tandon and Zahariev (2001, Appendix) who comment that in order to obtain useful formation rate estimates it is necessary to resolve the isopycnal meanders of the control surface.

4 Transformed Eulerian-mean (TEM) formalism

To what extent can we rephrase Walin’s water mass analysis formulation so that it might be used with “coarse-grained” estimates of outcrop windows and air-sea fluxes? Averaging results in a loss of information which must be recovered somehow. A natural way forward is to adopt a “Transformed Eulerian-Mean” (TEM) perspective in which advection of a mean tracer distribution is accomplished by a residual-mean velocity while residual (non-skew) eddy fluxes appear as forcing terms on the r.h.s. The residual flow is related to (in fact in a quasi-geostrophic, statistically steady state, equal to) the mass-weighted mean circulation in isopycnal coordinates (Andrews et al., 1987). It is the sum of the “eddy induced” — also known as the “quasi-Stokes” flow — and the Eulerian mean flow. The residual mean therefore yields the flow that transports mean tracer fields (such as heat, passive tracers, and active tracers such as potential vorticity) in an eddying ocean. See, for example, DM97, Marshall and Radko (2003), Kuo et al.(2005).

Specifically, we write the time-mean of the buoyancy equation (5) in the form:

$$\frac{\partial \bar{\sigma}}{\partial t} + \nabla \cdot (\mathbf{u}_{res} \bar{\sigma} + \mathbf{N}_{\bar{\sigma}} + \mathbf{N}_{\sigma_{res}}) = 0 \quad (15)$$

where \mathbf{u}_{res} is the residual flow and $\mathbf{N}_{\sigma_{res}} = (\overline{\mathbf{u}'\sigma'}) \cdot \hat{\mathbf{n}}_{\sigma}$ is the “residual eddy flux” — the flux that is not “skew” (Plumb and Ferrari, 2005). If $\overline{\mathbf{u}'\sigma'} \cdot \hat{\mathbf{n}}_{\sigma} = 0$ then $\mathbf{N}_{\sigma_{res}} = 0$ and the eddy flux divergence can be entirely represented as an advective process and subsumed in to \mathbf{u}_{res} . Otherwise there will always be a non-advective contribution associated with the eddies. DM97 has pointed out that eddy buoyancy flux within the mixed layer includes both advective and diffusive components, where the later are due to diabatic mixing along the sea surface. Therefore, the rate at which a water mass is subducted from the surface mixed layer into the ocean interior is determined by air-sea buoyancy flux and the diapycnal component of eddy buoyancy forcing (compare our Eqs. (15) and (16) with DM97 equations (14) through (16)). The contribution of the non-advective component of eddy buoyancy

flux has largely been neglected in previous studies. DM97 includes it when developing a theoretical framework for diagnosing the contribution of mesoscale eddies to the subduction of a water-mass. However, when applying the theory to the Southern Ocean circulation, DM97 neglects the diffusive component of eddy buoyancy flux, given by $\overline{\mathbf{u}'T'} \cdot \hat{\mathbf{n}}_T$, in the mixed layer. Marshall and Radko (2003) argue that the diffusive term is important in the Southern Ocean. What do we observe in our numerical simulation?

The zonal average temperature and eddy heat flux, Fig.14, shows that the ‘raw’ eddy flux is parallel to the isotherms everywhere in the channel except in the vicinity of the main jet and in the surface diabatic layer, just as found in Kuo et al.(2005). Kuo et al. (2005) estimate the depth of the surface diabatic layer in the presence of the mixed layer as the sum of the mean mixed layer depth and the maximum thickness of the ventilated layer given by $\sqrt{\overline{T'^2}}/\overline{T}_z$ where $\sqrt{\overline{T'^2}}$ is the eddy temperature perturbation at the surface and \overline{T}_z is the mean vertical temperature gradient at the base of the surface diabatic layer. We estimate that the depth of the surface diabatic layer is approximately 100 m in our calculation. Since the divergence of the diapycnal eddy heat flux is large in the surface layer (Fig.14, top panel, shows a poleward eddy heat flux), it is evident that $\mathbf{N}_{\sigma_{\text{res}}} \neq 0$ and so Eq.(8) will have a contribution due to eddies:

$$D_{\text{eddy}} = \int \int_{\text{diabatic zone}} \overline{\mathbf{u}'T'} \cdot \hat{\mathbf{n}}_T d\mathcal{A} , \quad (16)$$

where the residual flux is integrated over the temperature surface as it cuts through the surface diabatic zone. Here $\hat{\mathbf{n}}_T$ is unit vector pointing outward normal to the isotherms. When diagnosing D_{eddy} we neglect the small scale diffusive flux, which has already been shown to be very small (Section 3.3).

Fig.15 shows the zonally and time averaged residual eddy heat flux integrated over the outcropping temperature surface in the mixed layer, along with the zonally and time-averaged surface air-sea heat flux, both obtained from 100 years of model output. We see that the two terms oppose one-another over the whole latitude range. The residual heat flux is polewards

in the latitude range $10^{\circ}S$ to $15^{\circ}S$. The air-sea heat flux, on the other hand, is directed in to the ocean in this latitude range. Moreover, the magnitude of the eddy heat flux slightly exceeds that of the air-sea heat flux. Inspection of local balances shown in Fig.9 reveals that over most of the basin air-sea heat flux and eddy-induced heat flux are of comparable magnitude, but of the opposite sign. However, poleward of $14^{\circ}S$, in the region where the eddies are strong, eddy fluxes slightly exceed air-sea heat flux.

Fig.16 shows the results of a residual-mean Walin analysis performed on 100 years of annually-averaged model temperature data and eddy fluxes $\overline{\mathbf{u}'T'}$. In the temperature range from $21^{\circ}C$ to $25^{\circ}C$, residual eddy fluxes give rise to negative transformation rates. In the temperature range $19.5^{\circ}C$ to $21^{\circ}C$ lateral eddy transfer again slightly exceeds the magnitude of heat loss due to air-sea interaction, and induces positive transformation rates. This results in the formation of $0.25 \text{ Sv}/^{\circ}C$ of $21^{\circ}C$ water, lower than the actual formation rate but now, at least, of the correct sign.

The formation rate calculated using the TEM framework is different from the formation rate calculated using daily data, primarily because the use of daily data provides sufficient resolution in time to be able to follow the isopycnals, and so calculated formation rates are correctly assigned to the density interval where the formation occurs. When working in the TEM framework, on the other hand, the data have been averaged in time at a fixed position, so the calculated formation rates are estimated between the mean isopycnals. Since the isopycnals move around in space with time, formation that occurs in a certain density interval will become smeared over several neighboring density intervals.

5 Effect of strength of thermal coupling

How do our results depend on the magnitude of the air-sea coupling parameter? Cox (1985) and Boening and Budich (1991) showed that large-scale ocean circulation exhibits compensation between $\overline{\mathbf{u}} \cdot \nabla \overline{\mathbf{T}}$ and $\nabla \cdot (\overline{\mathbf{u}'T'})$ in eddy permitting numerical model simulations. Drijfhout and Walsteijn (1998) showed that the degree of compensation depends critically

on the strength of the air-sea coupling and that the result of Cox (1985) and Boening and Budich (1991) may be a consequence of inadequate air-sea interaction i.e. too weak thermal coupling between the atmosphere and the ocean on the eddy scale.

Huang (1989) suggested that the strength of thermal driving can be expressed by the nondimensional parameter Γ , which is the ratio of the advection time and the relaxation time of the upper layer temperature field toward surface air temperature:

$$\Gamma = L/(U\tau) \tag{17}$$

where L is a representative length scale, U is the advection velocity and τ is the relaxation time scale. Thus if Γ is small, diabatic effects are small compared to advective ones and the air-sea coupling is weak. In this limit one might expect to observe compensation between mean and eddy heat transport, as discussed in Drijfhout, 1994. In the experiment reported here, the appropriate length scale is that of the eddy itself; eddy filaments are advected around the “mode one” eddy in approximately 10 days. Thus $L \approx 1000 \text{ km}$ (the distance over which eddies advect filaments), $U \approx 3\text{-}4 \text{ m/s}$ (a typical velocity by which filaments are advected), and $\tau = 30 \text{ day}$, giving a $\Gamma \approx 0.13$ and suggesting that compensation ought indeed to be observed in our experiment. Note however that we cannot directly compare our estimate with quoted values for Γ since the coupling depends on the details of the oceanic and atmospheric flow configuration (Drijfhout, 1994b).

In ocean-only models, thermal coupling coefficients are tuned to match typical SST-air temperature anomalies at the scale of 1000 km. Drijfhout (1994) has suggested that the thermal coupling at the eddy scale would undergo a transition between weak and strong coupling when the thermal coupling coefficient becomes larger than about $100 \text{ W m}^{-2} \text{ K}^{-1}$. The thermal coupling coefficient appropriate to our calculation may be found by differentiating Eq.(1) wrt T to yield: $\frac{\partial \mathcal{H}}{\partial T} = -\frac{\rho c_w d_1}{\tau}$ or, inserting numbers, $13 \text{ W m}^{-2} \text{ K}^{-1}$ (cooling if SST increases). This confirms that with $\tau = 30 \text{ day}$, our experiment is in the weak coupling limit: eddy filaments can be advected large meridional distances without significant change in temperature and so find themselves in regions where they are much warmer than

the air above. Heat is thus lost to the atmosphere, triggering convection and giving rise to subduction of low PV water.

To see what happens when coupling is stronger we reran the numerical simulation with a relaxation time of 6 days, which yields a Γ of about 0.7. The most important result is that the temperature of eddy filaments quickly becomes almost indistinct from that of the surrounding water. Moreover, with stronger coupling, the eddy field is smoother and there is considerably less filamentation (Figure 13, top panel). The meridional distribution of sea-surface temperature is more uniform, as is the air-sea heat flux. The strongest air-sea heat exchange is due to the effects of horizontal mixing and stirring caused by the “mode one” eddy, so the typical air-sea heat flux pattern shows the ocean gaining heat in the equatorward half of the “mode one” eddy and losing heat in the poleward half of the “mode one”. This pattern is somewhat similar to time-averaged air-sea heat flux from the weak coupling case, but the instantaneous heat flux pattern shows less correlation with filaments than in the weaker coupling case.

The strong coupling transformation rate promotes ocean heat loss in the poleward half of “mode one” eddy, transforming water over broader temperature ranges and larger surface outcrop areas, resulting in enhanced low PV water formation rate (Figure 13, bottom panel, shows that 4 Sv of water is formed when analyzed one year of daily data). This is in agreement with the results of Drijfhout (1994a) and of Drijfhout and Walsteijn (1998) who found that there is less compensation between eddy and mean flow transport in the case of strong coupling. Comparison of Figures 5 and Figure 13, (top panels) as well as Figure 12 and Figure 13 (lower panels) confirms that water mass formation, being determined by air-sea heat exchange, depends crucially on the strength of thermal coupling.

6 Discussion and conclusions

The effects of eddy modulation of air-sea interaction and convection on the process of mode water formation have been studied in a baroclinically unstable wind- and buoyancy-driven

model flow in a pie-shaped sector of the sphere. Walin’s (1982) analysis has been used to estimate formation rates in the presence of eddies and to characterize the role of eddies in that process. In an ideal world, water mass formation would be computed using synoptic outcrop fields and synoptic air-sea fluxes (Garrett and Tandon, 1997; DM97). We therefore first performed Walin’s analysis using model data with sufficient resolution in space and time to capture the eddies. The result (Fig.11) shows a pronounced peak in the formation rate in the appropriate temperature range, corresponding to that of the water that feeds the low PV pool (see Fig.6). However, when formation rates are estimated from temperature and heat flux data that have been averaged in time at a fixed location, they yield erroneous formation rates. The large difference between the formation rate estimates obtained from synoptic data which resolve the eddies and time averaged data which do not resolve them, point to the fundamental importance of including eddy effects in the analysis.

Taking covariances describing the eddy effects into account, which we have done by adopting TEM framework with allowance for eddy fluxes for the Walin analysis, significantly improves matters. In our numerical simulation, residual eddy heat fluxes and air-sea fluxes are found to play a comparable role in setting the transformation. They are of the opposite sign and nearly cancel each other. A heat budget rephrased in terms of TEM shows that this is to be expected if the residual circulation is weak, as in the flow analyzed here. In our calculation the eddy-induced mean flow tends to balance the Eulerian-mean flow over most of the basin. Because of this near cancellation, water mass formation estimates based on non-synoptic air-sea heat flux data and outcrops may “miss” one of the two dominant heat transfer mechanisms and hence yield formation rates which are very much in error, as summarized in the following modified Walin balance:

$$A_{res} = \underbrace{A_{mean} + A_{eddy}}_{\text{partial cancellation}} = \underbrace{F_{air-sea} - \frac{\partial D_{eddy}}{\partial \sigma}}_{\text{partial cancellation}} \quad (18)$$

Note that eddy terms appear on both sides of the equation. The diapycnal volume flux in a turbulent ocean has a contribution from the eddy-induced transport A_{eddy} which, as

in the calculations presented here, largely cancels A_{mean} . This is certainly true in strong frontal regions such as the Antarctic Circumpolar Current. For example, the vanishing of the “Deacon Cell” in the Southern Ocean is a case in point where equatorward Ekman transport is largely balanced by poleward eddy-induced transport – see, e.g., Danabasoglu et al. (1994), Doos and Webb (1994), McIntosh and McDougall (1996) and Karsten and Marshall (2002). So, not only may $\frac{\partial D_{eddy}}{\partial \sigma}$ partially cancel $F_{air-sea}$, but also A_{mean} and A_{eddy} tend to compensate one-another. In the conventional application of air-sea flux analyses to water mass formation estimates — as in, for example, Speer and Tziperman (1992) — A_{mean} is set equal to $F_{air-sea}$, resulting in a likely erroneous estimate of formation rates in the vicinity of fronts, where D_{eddy} and A_{eddy} are important.

In the experiments presented here, mode water is formed when near-surface water parcels are displaced large meridional distances in filamentary structures associated with the eddies. Large air-sea temperature differences, and hence vigorous air-sea interaction are induced, which triggers convection and the creation of low potential vorticity water. Because of the simple geometry adopted in our model, eddy processes are the only mechanism at work driving disequilibrium between the atmosphere and the ocean. In the ocean, however, water is also displaced from its equilibrium latitude by the mean flow, in western boundary currents and jets, a process which is absent from our model. This is a key process in the formation of, for example, EDW, the subtropical mode water of the Atlantic. Therefore in a system like the Gulf Stream mode water can also be formed in the absence of eddies. Indeed, coarse resolution models show mode water formation (e.g. Hazeleger and Drijfhout, 1998, 1999; Marsh and New, 1996; Paiva and Chassignet, 2002). It remains to be seen whether the role of eddies in mode water formation explored here is a true reflection of the role played by eddies in nature.

Acknowledgements. IC acknowledges support from NSF, under grant OCE-0426307. IC would like to thank Leif Thomas for motivating discussions and insightful comments on the early draft. We would also like to thank two anonymous reviewers for suggesting im-

provements to the text. JM was supported by an NSF OCE grant supporting the CLIMODE project.

References

- Andrews, D. G., J. R. Holton and C. B. Loevy, 1987: Middle Atmosphere Dynamics. *Academic Press*, 489 pp.
- Boening, C. W. and R. G. Budich 1992: Eddy Dynamics in a Primitive Equation Model: Sensitivity to Horizontal resolution and Friction. *J. Phys. Oceanogr.*, **22**, 361-381.
- Cerovečki I., R. A. Plumb and W. Heres, 2006: Eddy transport and mixing in a wind and buoyancy driven jet on the sphere. (*J. Phys. Oceanogr.*, *sub judice*).
- Cox, M. D. 1985: An Eddy Resolving Numerical Model of the Ventilated thermocline. *J. Phys. Oceanogr.*, **15**, 1312-1324.
- Danabasoglu, G., J. C. McWilliams, and P. R. Gent, 1994: The role of mesoscale tracer transport in the global ocean circulation. *Science*, **264**, 1123-1126.
- Dewar, W. K., 1986: On the potential vorticity structure of weakly ventilated isopycnals: A theory of subtropical mode water maintenance. *J. Phys. Oceanogr.*, **16**, 1204-1216.
- Dong, S. and K. A. Kelly, 2004: Heat budget in the Gulf Stream region: the importance of heat storage and advection. *J. Geophys. Res.*, **99**, 18481-18499.
- Donners, J., S. S. Drijfhout and W. Hazeleger, 2005: Water Mass Transformation and Subduction in the North Atlantic. *J. Phys. Oceanogr.*, **35**, 1841-1860.
- K. Doos and D. J. Webb, 1994: The Deacon Cell and Other Meridional Cells of the Southern Ocean. *J. Phys. Oceanogr.*, **24**, 429-442.
- Drijfhout, S. S. 1994a: Heat transport by Mesoscale Eddies in an Ocean circulation Model. *J. Phys. Oceanogr.*, **24**, 353-369.
- Drijfhout, S. S. 1994b: Sensitivity of eddy-induced heat transport to diabatic forcing. *J. Geophys. Res.*, **99**, 18,481–18,499.
- Drijfhout S. S. and F. H. Walsteijn, 1998: Eddy-Induced heat Transport in a Coupled Ocean-Atmosphere Anomaly Model. *J. Phys. Oceanogr.*, **28**, 250-265.
- Ebbesmeyer, C. C. and E. J. Lindstrom, 1986: Structure and origin of 18 ° water observed during POLYMODE Local Dynamics Experiment. *J. Phys. Oceanogr.*, **16**, 443-453.

- Garrett, C., K. Speer and E. Tragou, 1995: The relationship between water mass formation and the surface buoyancy flux, with application to Phillips' Red Sea model. *J. Phys. Oceanogr.*, **25**, 1696-1705.
- Garrett, C., A. Tandon, 1997: The effects on water mass formation of surface mixed layer time-dependence and entrainment fluxes. *Deep Sea Research*, **44/12**, 1991 - 2006.
- Hazeleger W. and S. S. Drijfhout, 1998: Mode water variability in a model of the subtropical gyre: Response to anomalous forcing. *J. Phys. Oceanogr.*, **28**, 266-288.
- Hazeleger W. and S. S. Drijfhout, 1999: Stochastically forced mode water variability. *J. Phys. Oceanogr.*, **29**, 1772-1786.
- Hazeleger W. and S. S. Drijfhout, 2000: Eddy Subduction in a Model of the Subtropical Gyre. *J. Phys. Oceanogr.*, **30**, 677-695.
- Huang, R. X., 1989: Sensitivity of a multilayered oceanic general circulation model to the sea surface thermal boundary condition. of the Subtropical Gyre. *J. Geophys. Res.*, **94**, 18,011–18,021.
- Jenkins, W. J., 1982: On the climate of a subtropical ocean gyre: Decade timescale variations in water mass renewal in the Sargasso Sea. *J. Mar. Res.*, **40** (Supplement), 265-290.
- Karsten, R. and J. Marshall 2002: Constructing the residual circulation of the Antarctic Circumpolar Current from observations. *J. Phys. Oceanogr.*, **32**, 3315-3327.
- Kelly, K.A., 2004: The relationship between oceanic heat transport and surface fluxes in the western North Pacific: 1970-2000. *J. Clim.*, **17**, 573-588.
- Klinger, B.A., J. Marshall, and U. Send, 1996: Representation and parameterization of deep convective plumes by mixing. *J. Geophys. Res.*, **101**, 18175-18182.
- Kuo, A., R. A. Plumb, and J. Marshall, 2005: Transformed Eulerian mean theory. II: Potential vorticity homogenization, and the equilibrium of a wind- and buoyancy-driven zonal flow. *J. Phys. Oceanogr.*, **35**, 175-187.
- Kwon, Y.-O., S.C. Riser, 2005a: The Eighteen Degree Water of the North Atlantic Observed Using Profiling Floats *J. Phys. Ocean.*, submitted.

Kwon, Y.-O., S.C. Riser, 2005b: The General Circulation of the Western Subtropical North Atlantic Observed by Using Profiling Floats. *J. Geophys. Res.*, submitted.

Marsh and New, 1996: Modeling 18 Water Variability. *J. Phys. Oceanogr.*, **26**, 1059-1080.

Marshall, D., 1997: Subduction of water masses in an eddying ocean. *J. Mar. Res.*, **55**, 201-222.

Marshall, J., D. Jamous and J. Nilsson, 1999: Reconciling “thermodynamic” and “dynamic” methods of computation of water-mass transformation rates. *Deep-Sea Res. I*, **46**, 545-572.

Marshall, J., C. Hill, L. Perleman and A. Adcroft, 1997a: Hydrostatic, quasi-hydrostatic, and non hydrostatic ocean modeling. *J. Geophys. Res.*, **102**, 5753-5766.

Marshall, J., C. Hill, L. Perleman and C. Heisy, 1997b: A finite volume, incompressible Navier-Stokes model for studies of the ocean on parallel computers. *J. Geophys. Res.*, **102**, 5753-5766.

Marshall, J., and T. Radko, 2003: Residual-mean solutions for the Antarctic Circumpolar Current and its associated overturning circulation. *J. Phys. Oceanogr.*, **33**, 2341-2354.

Large, W. G., J. C. McWilliams and S. C. Doney, 1994: Oceanic vertical mixing: a review and a model with a nonlocal boundary layer parameterization. *Rev. of Geoph.*, **32**, 363-403.

McCartney, M. S., 1982: The subtropical recirculation of Mode Waters. *J. Mar. Res.*, **40** (Supplement), 427-464.

McIntosh P. C., and T. J. McDougall, 1996: Isopycnal Averaging and the Residual Mean Circulation. *J. Phys. Oceanogr.*, **26**, 1655-1660.

Paiva A. M. and E. P. Chassignet 2002: North Atlantic modeling of low-frequency variability in mode water formation. *J. Phys. Oceanogr.*, **32**, 2666-2680.

Panetta, R. L. 1993: Zonal Jets in Wide Baroclinically Unstable Regions: Persistence and Scale Selection. *J. Atmos. Sci.*, **50**, 2073-2106.

Plumb, R.A., and R. Ferrari, 2005: Transformed Eulerian-Mean Theory. Part I: Nonquasi-geostrophic Theory for Eddies on a Zonal-Mean Flow. *J. Phys. Oceanogr.*, **35**, 165-174.

Rhines, P. B., 1994: Jets, *Chaos*, **4**, Amer.Inst.of Physics, 313-341.

- Speer K. and E. Tziperman, 1992: Rates of water mass formation in the North Atlantic. *J. Phys. Oceanogr.*, **22**, 93-104.
- Schroeder E. H., H. Stommel, D. W. Menzel and W. J. Sutcliffe, 1959: Climate stability of eighteen degree water at Bermuda. *J. Geophys. Res.*, **64**, 363-366.
- Tandon A., and K. Zahariev, 2001: Quantifying the role of mixed layer entrainment for water mass transformation in the North Atlantic. *J. Phys. Oceanogr.*, **31**, 1120-1131.
- Talley L. D. and M. E. Raymer, 1982: Eighteen Degree Water variability. *J. Mar. Res.*, **40** (Supplement), 725-775.
- Walín G., 1982: On the relation between sea-surface heat flow and thermal circulation in the ocean. *Tellus*, **34**, 187-195.
- Worthington L. V., 1959: The 18 ° water in Sargasso Sea. *Deep-Sea Res.*, **5**, 297-305.
- Worthington L. V., 1976: On the North Atlantic circulation. *John Hopkins Oceanographic studies*, **6**.

7 Figures

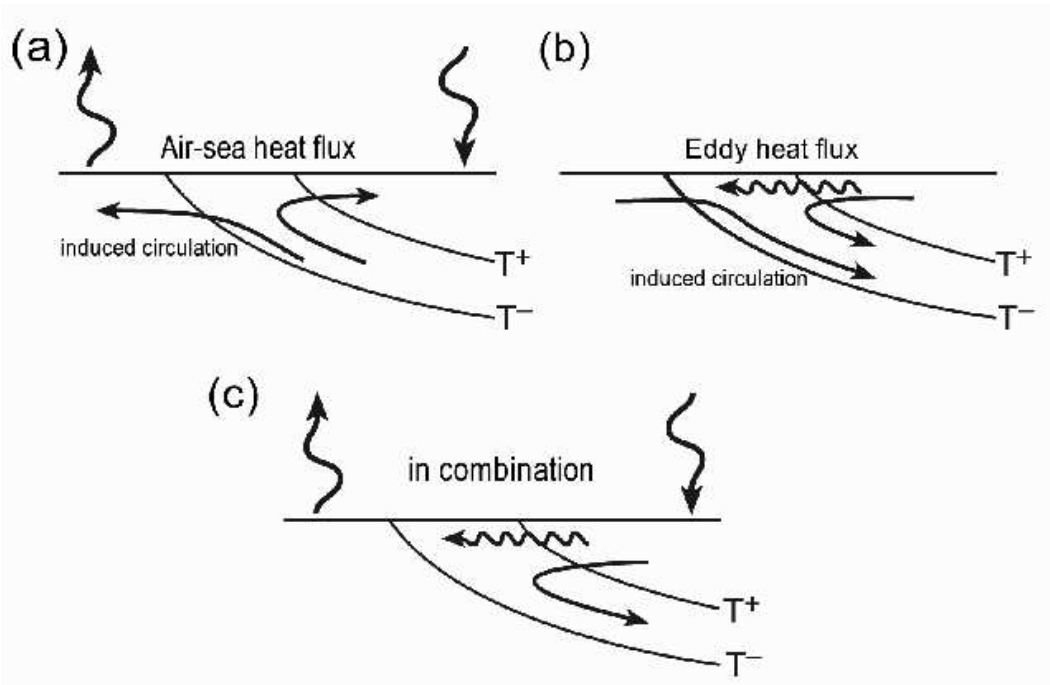


Figure 1: Illustration of eddy modulation of air-sea interaction in an idealized unstable frontal region with warm water on one side of the front and cold water on the other side, which get mixed across the front by eddies. Schematic of diapycnal volume flow induced by air-sea heat flux (upper left panel), diapycnal volume flow induced by eddy heat flux (upper right panel) and their sum (bottom panel) in the case when eddy heat flux exceeds air-sea heat flux. Wiggly arrows indicate the direction of the heat flux.

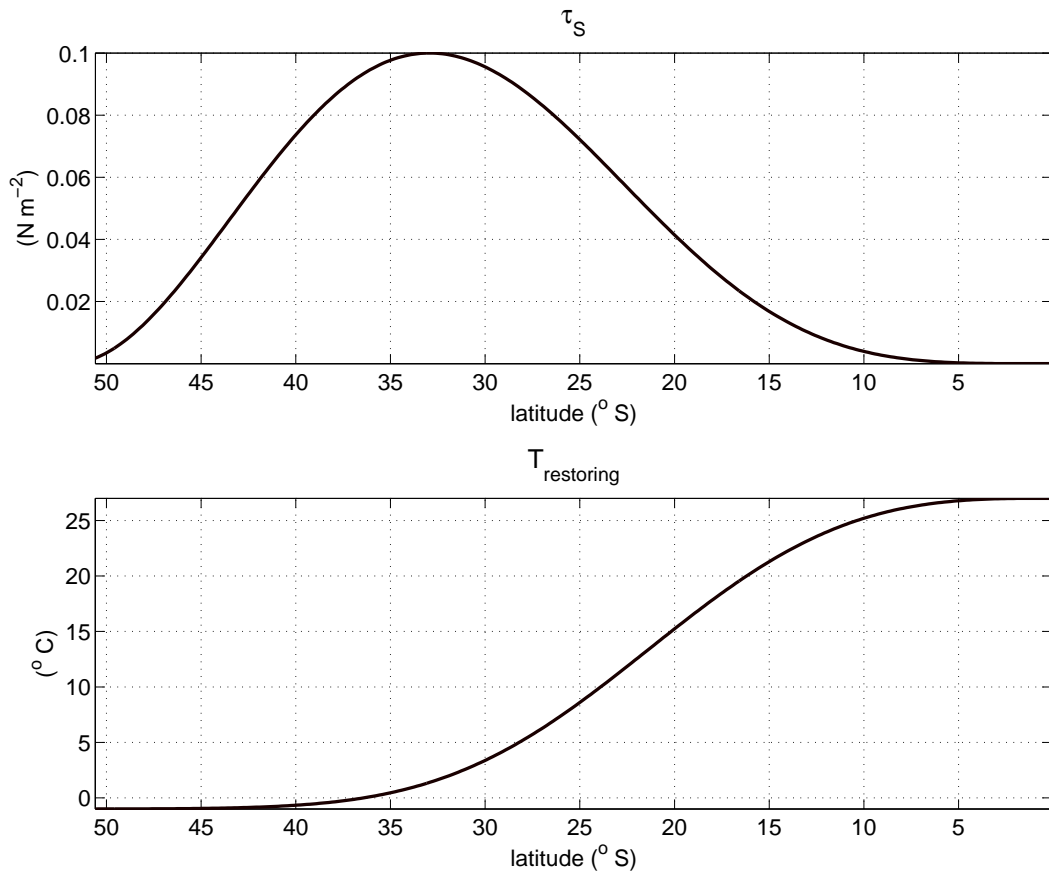


Figure 2: The wind stress forcing τ_S in N/m^2 and the restoring temperature in $^{\circ}\text{C}$. The restoring time scale in Eq.(1) is one month.

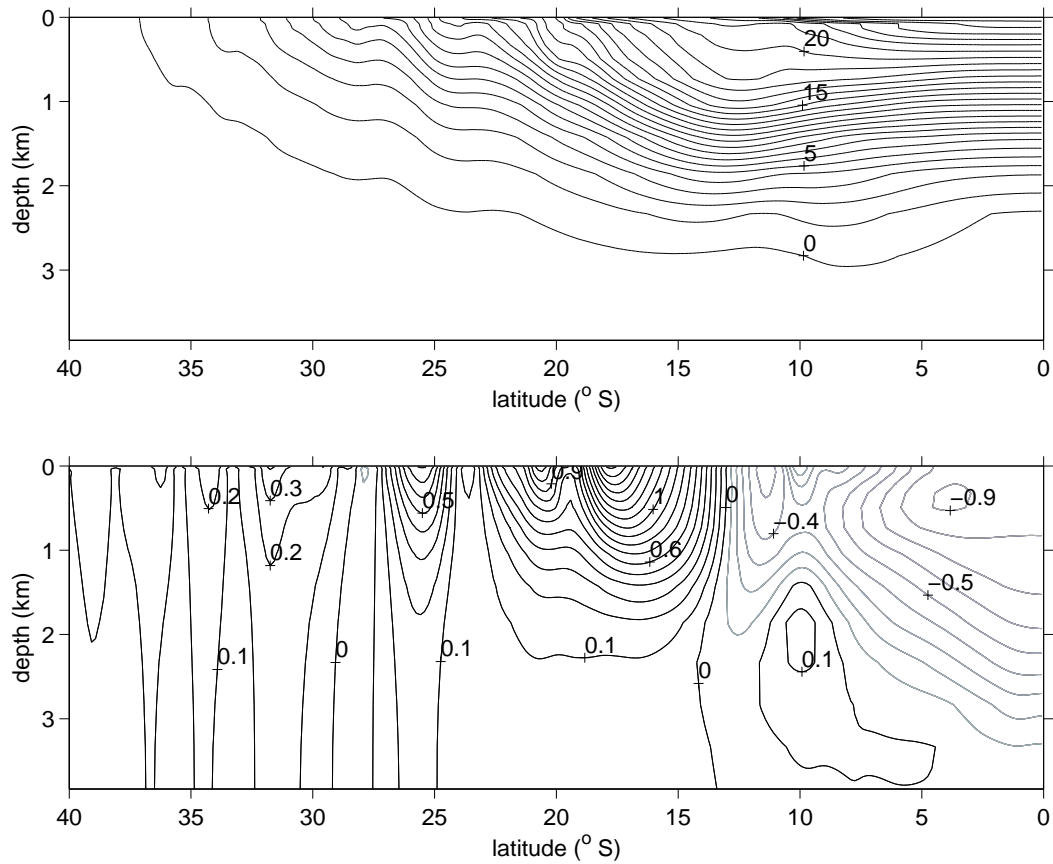


Figure 3: Top panel: instantaneous snap-shot of zonal mean temperature (in $^{\circ}\text{C}$). Note the low potential vorticity pool evident in the spreading of isotherms from 21°C to 19°C , located between 10°S and 15°S latitude at depths 100 m to 800 m. Bottom panel: instantaneous snap-shot of zonal mean zonal velocity for the same time, after 756 years of integration (in m/s).

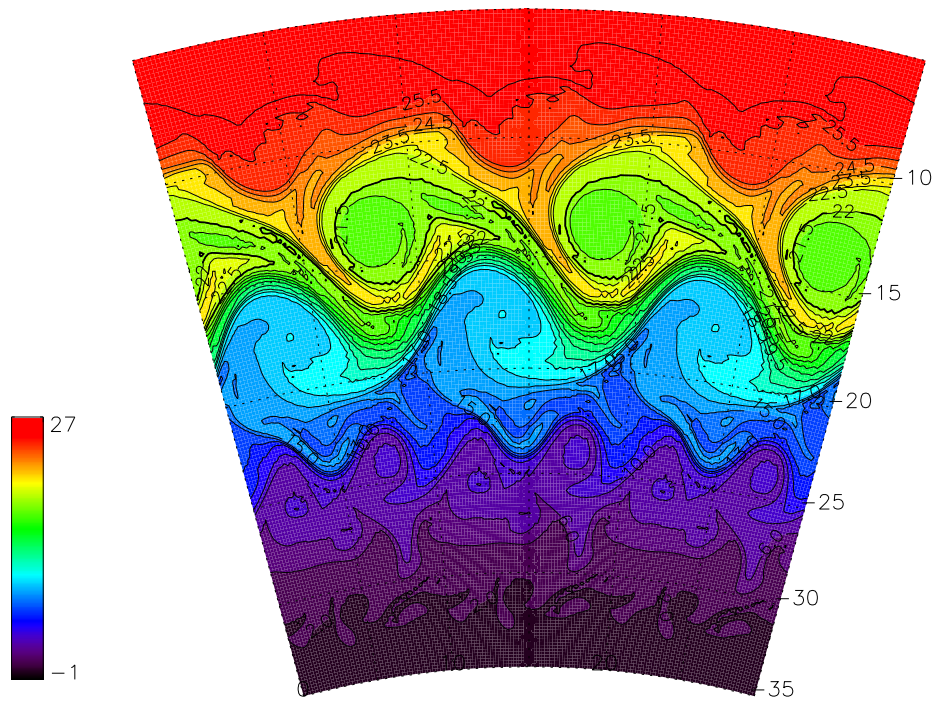


Figure 4: A snap shot of sea surface temperature ($^{\circ}\text{C}$); the periodic field is plotted three times in longitude, and only latitudes between 5°S and 35°S are shown). Thick line indicates 22°C isotherm.

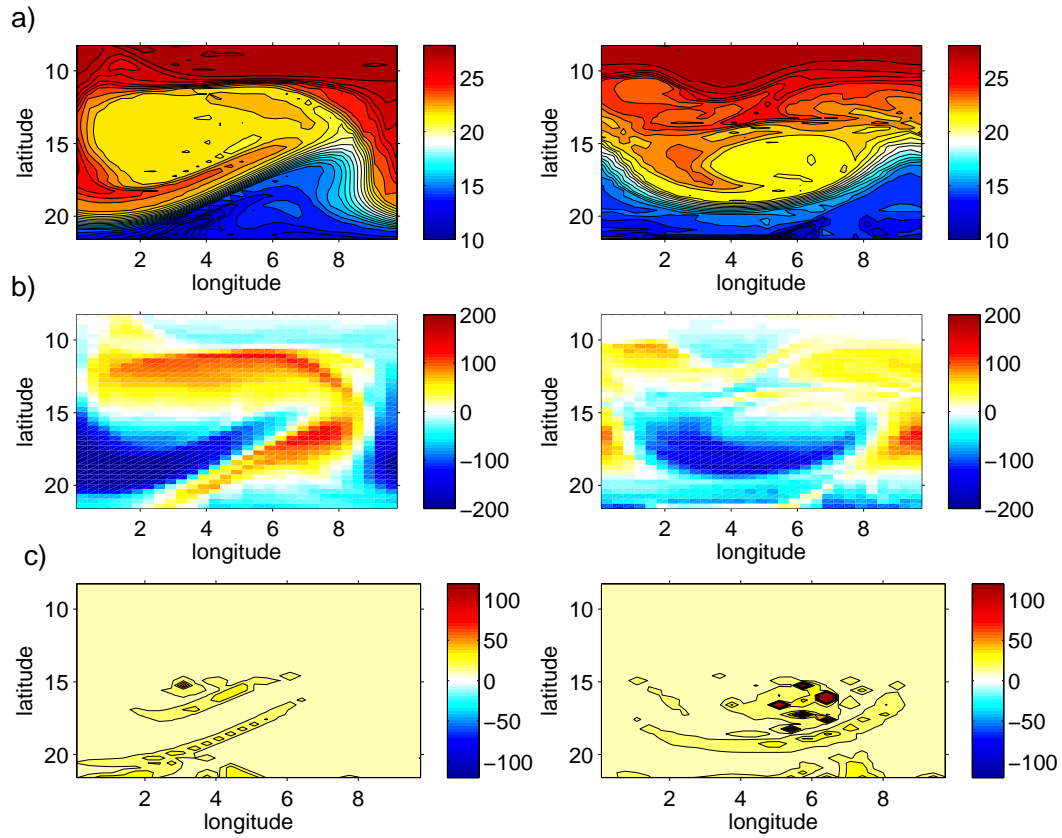


Figure 5: Synoptic maps of sea surface temperatures ($^{\circ}\text{C}$) with contour interval 0.5°C , heat flux (W m^{-2}) and mixing layer depth with contour interval 10 m, obtained from KPP parameterization, 22 days apart. Negative heat flux is out of the ocean.

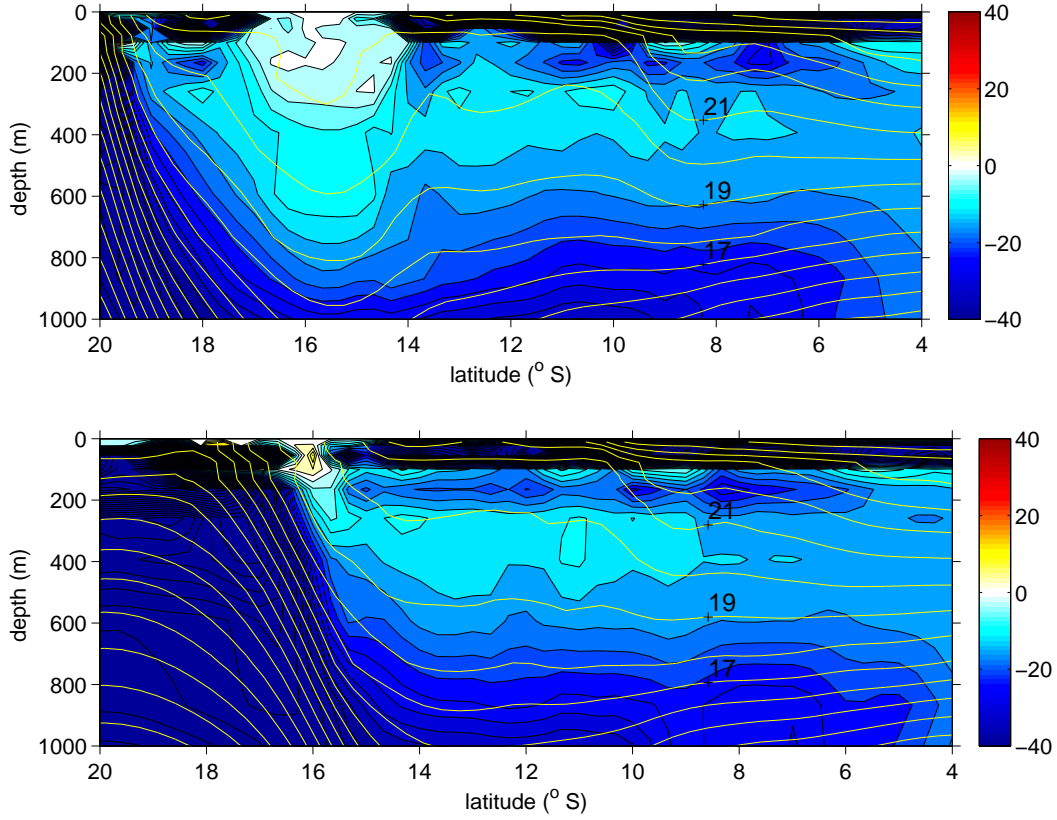


Figure 6: Snap-shot (daily averaged) of Ertel PV obtained as $\overline{PV} = \overline{\zeta_a \cdot \nabla T}$ (filled color contours, in $10^{-8} [^{\circ}\text{C m}^{-1} \text{s}^{-1}]$) and isopycnals (light lines, which coincide with the isotherms, in $^{\circ}\text{C}$) for fixed longitude 5° . Top panel shows a typical convective episode around 16°S generating low PV fluid feeding low PV pool (characterized by small negative and positive values of PV, indicated by light shades), and bottom panel shows low PV water spreading in the interior, 91 days later.

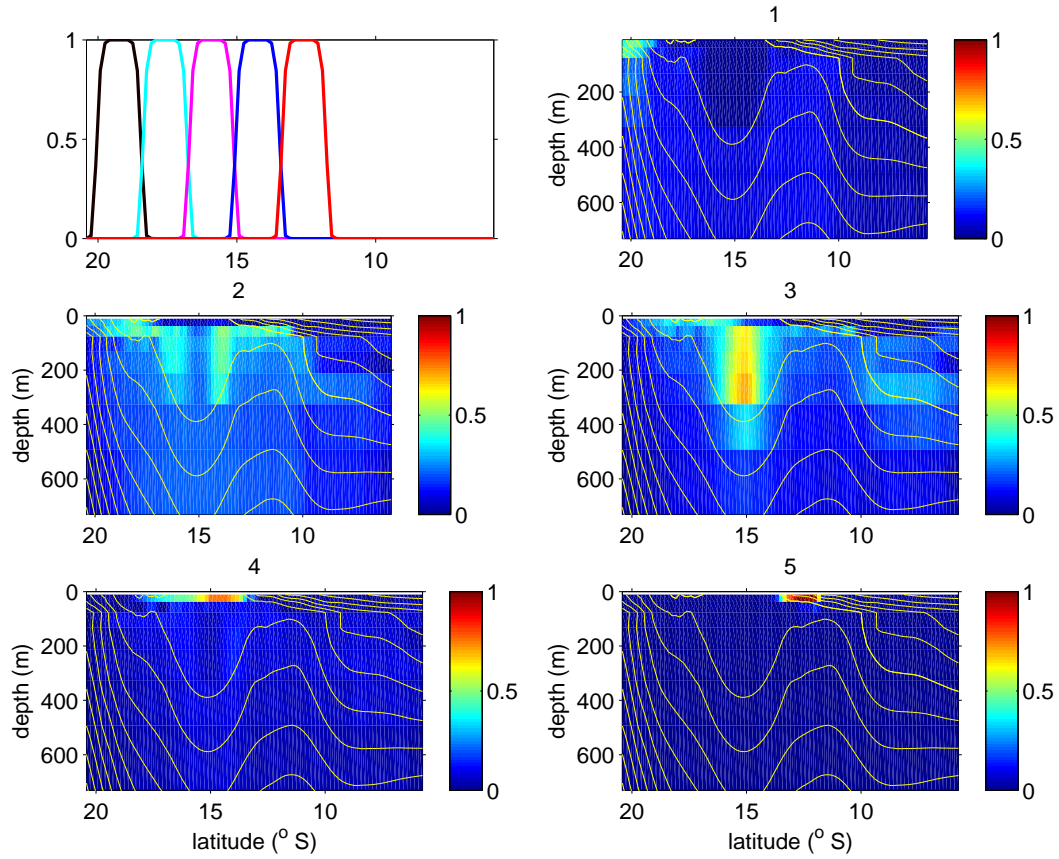


Figure 7: Meridional distribution from five tracer releases; in each the tracer concentration in the uppermost layer is restored to a specified distribution independent of the zonal direction and meridionally distributed as shown in first panel with a relaxation time of three days. (Tracer profiles in this subpanel are labeled one through five from left to the right). Remaining panels show tracer concentration for each release for longitude $x = 5^\circ$ after 30 years.

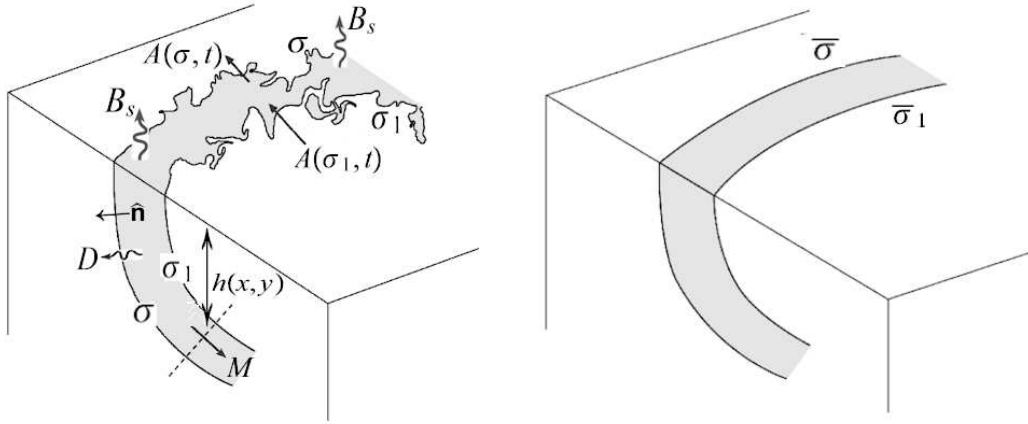


Figure 8: Schematic showing application of the formalism due to Walin (1982): Left panel shows the case of fine resolution model, which resolves meandering of the isotherms due to the presence of the eddies. The shaded region $R(\sigma, t)$ is bounded laterally by two outcropping isopycnals with density σ and reference density σ_1 , (less than σ) and vertically by the sea surface and a control surface $z = -h(x, y)$. Lateral volume flow $A(\sigma, t)$ across the isopycnals, whose convergence drives net subduction M across the control surface $h(x, y)$ in the ocean interior, is induced by air-sea density flux B_S acting across the sea surface and the interior density flux D , acting across the lateral isotherms. $\hat{\mathbf{n}}_\sigma$ is the unit vector perpendicular to the isopycnals. Right panel shows the corresponding picture in a coarse resolution model, which spatially smooths out both the lateral isopycnals and the outcropping window bounded by $\bar{\sigma}$ and $\bar{\sigma}_1$.

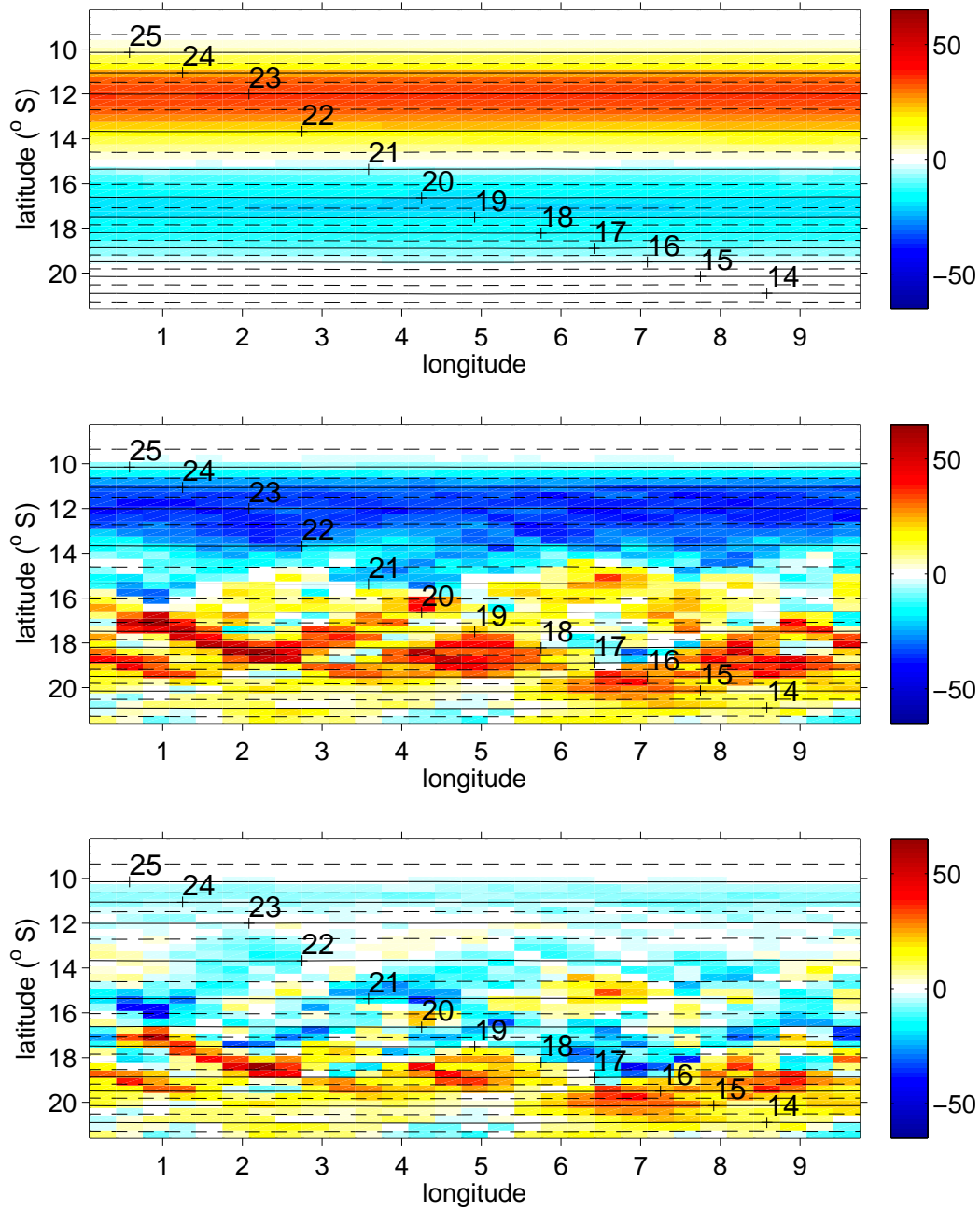


Figure 9: (Top) Air-sea heat flux H , (middle) vertically integrated diapycnal eddy heat flux divergence given by Eq.(16),(bottom) and their sum. Plots are time averaged over 100 years and are in Wm^{-2} . Air-sea fluxes which are warming the ocean are positive. The zonal average of each panel is shown in Fig.15. In all panels, black lines are contours of SST time averaged over 100 years.

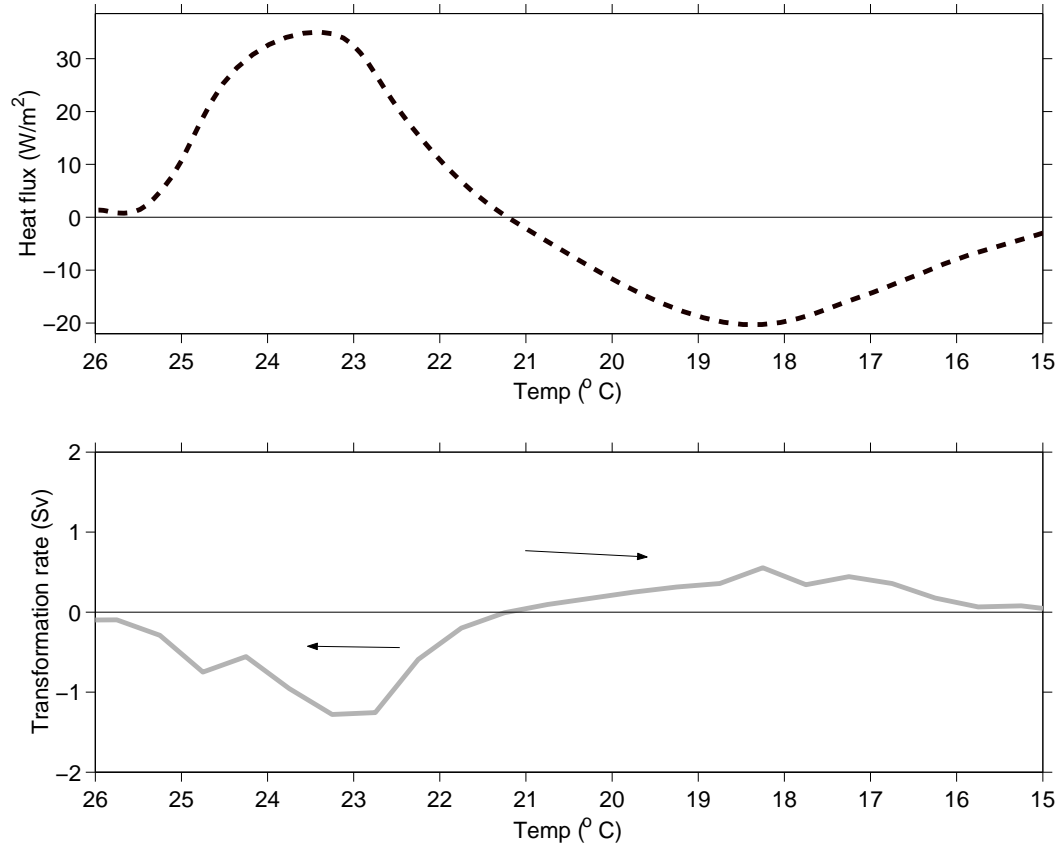


Figure 10: Results obtained by performing the Walin analysis on 100 years of annually and zonally averaged model SST data. Top panel: the air-sea heat flux (W/m^2) obtained from Eq. (1) using 100 years of annually and zonally averaged model SST data; also shown plotted against latitude in the top panel of Fig.9. Bottom panel: the diapycnal volume flux A diagnosed from Eq.(8) with “interior contributions” $\partial D/\partial T$ in Eq.(8) neglected and with B_s in Eq.(9) determined from the heat flux of the top panel via Eqs.(10) and (13).

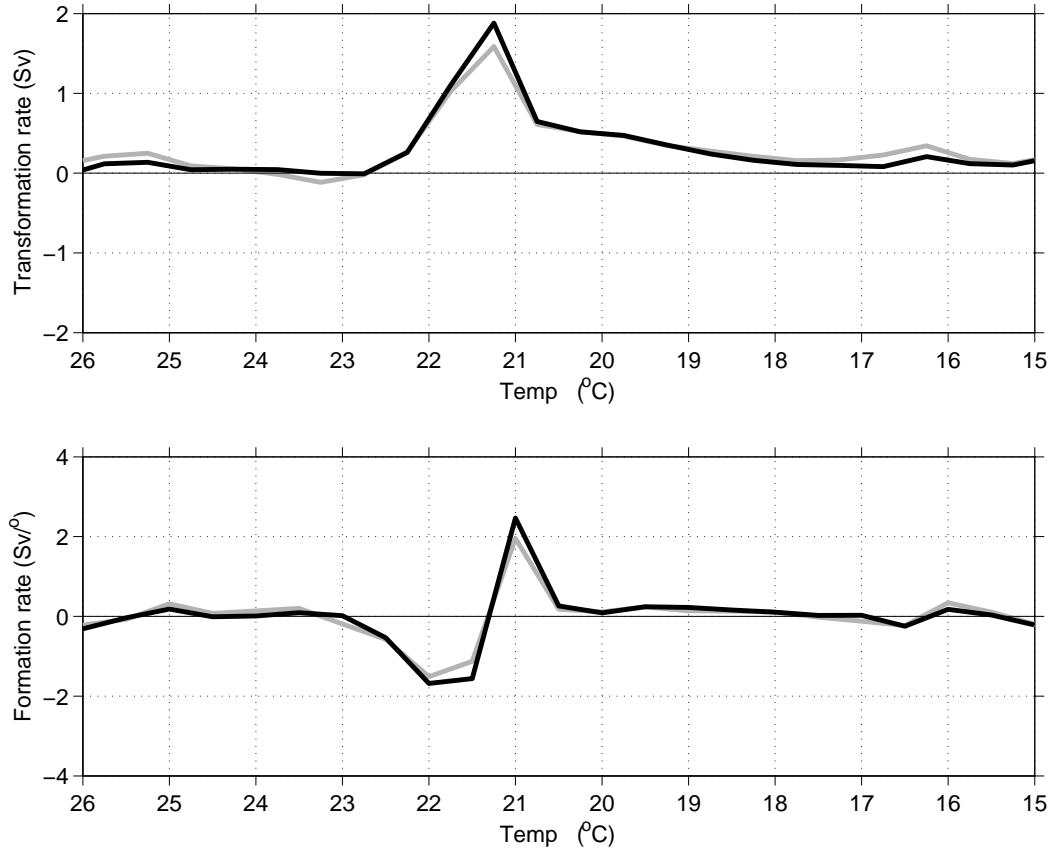


Figure 11: Top panel: volume flow A across the isotherms (in Sv) obtained performing the Walin analysis on 1 year of daily data using Eq.(8) (grey line) and taking into account only the air-sea heat flux in Eq.(8) (black line). The comparison shows that the contribution of the diffusive heat flux acting across the isotherms is small. Bottom panel: the corresponding formation rates estimated as $\partial A/\partial T$.

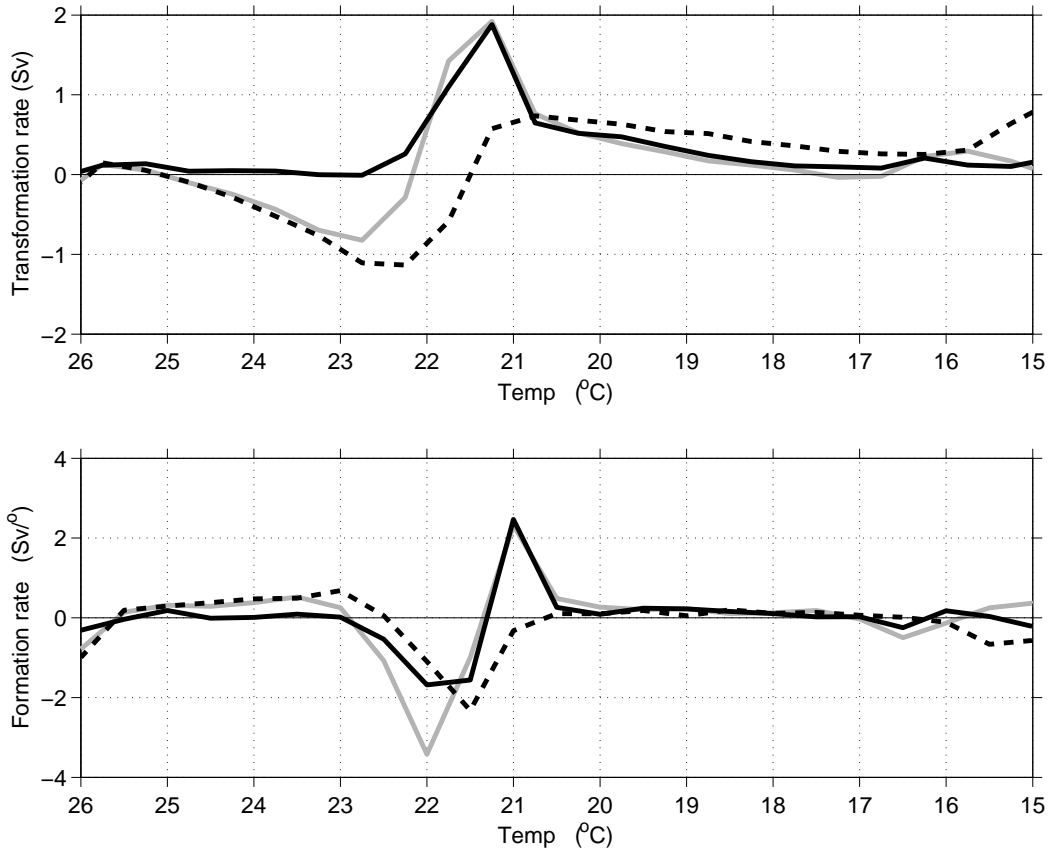


Figure 12: Transformation rate obtained by neglecting diffusive heat flux acting across the isotherms, D , so Eq.(8) reduces to $A = F_{air-sea}$, (A in Sv) and formation rate obtained as $\partial A / \partial T$ using 1 year of data in the Walin analysis. Black solid line shows results obtained from analyzing daily data, grey line shows results obtained using monthly temperature time averages to define both the outcrop windows as well as the air sea heat flux (using Eq.10) and dashed line shows results obtained using the annually averaged temperature to define both the outcrop windows and the air sea heat flux.

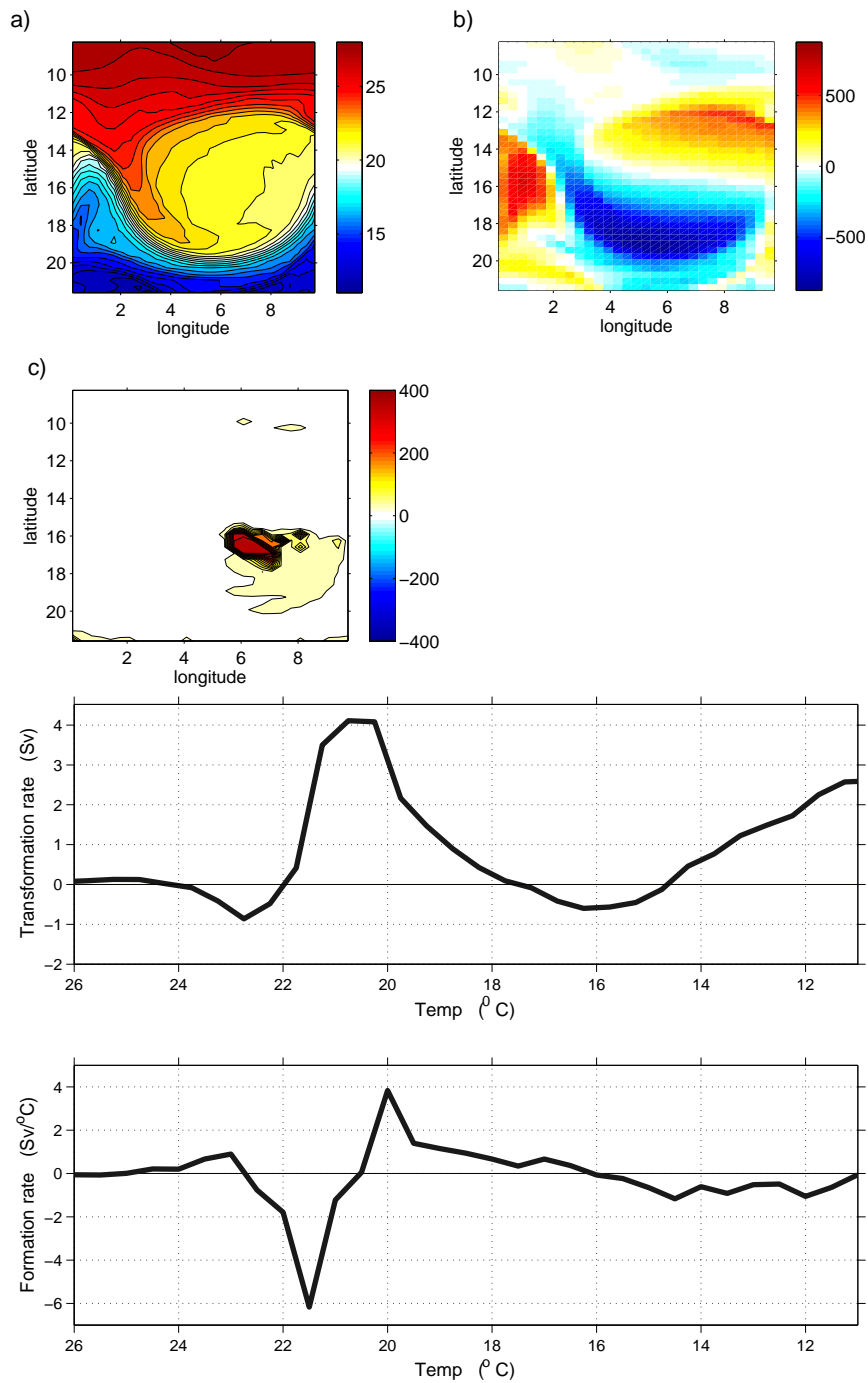


Figure 13: Results from a numerical experiment in which strong thermal coupling was employed (relaxation time of 6 days). Top panels: synoptic maps of (a) SST with contour interval 0.5°C , (b) heat flux (W m^{-2}) and (c) mixing layer depth with contour interval 25 m. Bottom panels: transformation rate obtained from $A = F_{air-sea}$, (A in Sv) and formation rate using 1 year of daily air sea heat flux data and daily estimates of outcrop windows in the Walin analysis.

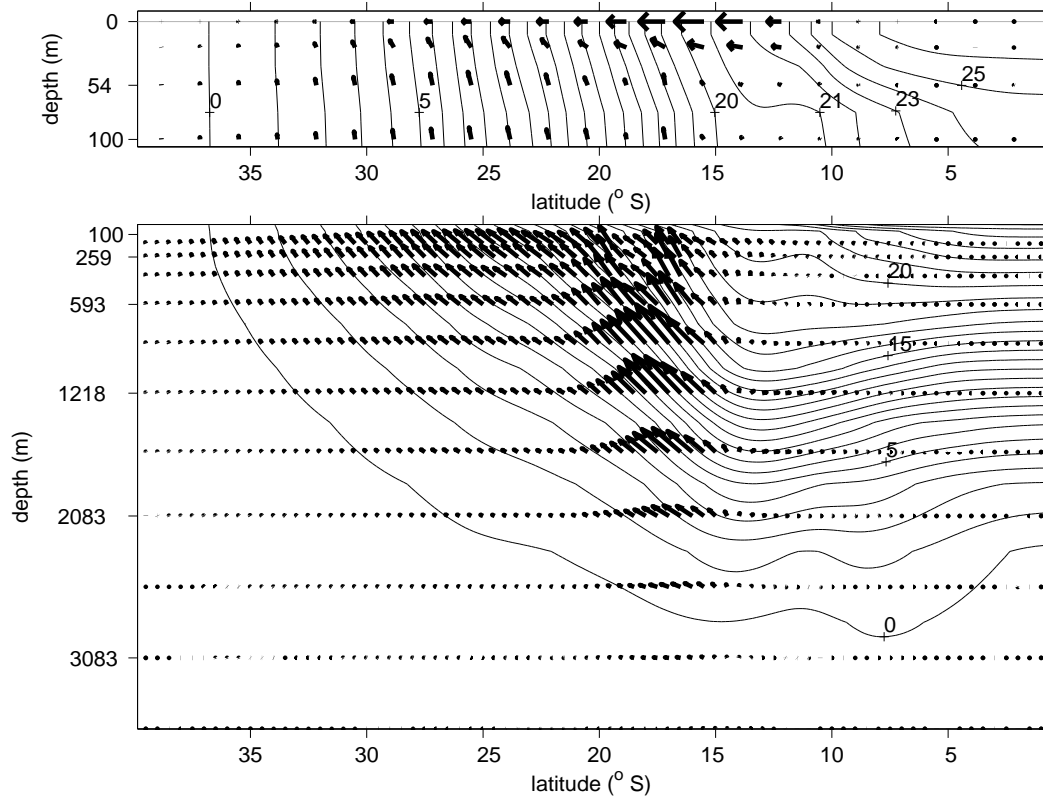


Figure 14: Meridional cross section of zonally averaged mean isopycnals which coincide with the mean isotherms (solid line, in $^{\circ}\text{C}$) and zonally and time averaged eddy temperature flux $\overline{\mathbf{u}'T'}$ (arrows); top panel shows the surface diabatic layer where the longest arrow corresponds to a flux of $0.15\text{ }^{\circ}\text{C m/s}$; bottom panel shows the near-adiabatic interior, where the longest arrow corresponds to a flux of $0.02\text{ }^{\circ}\text{C m/s}$. Light solid line indicates the surface.

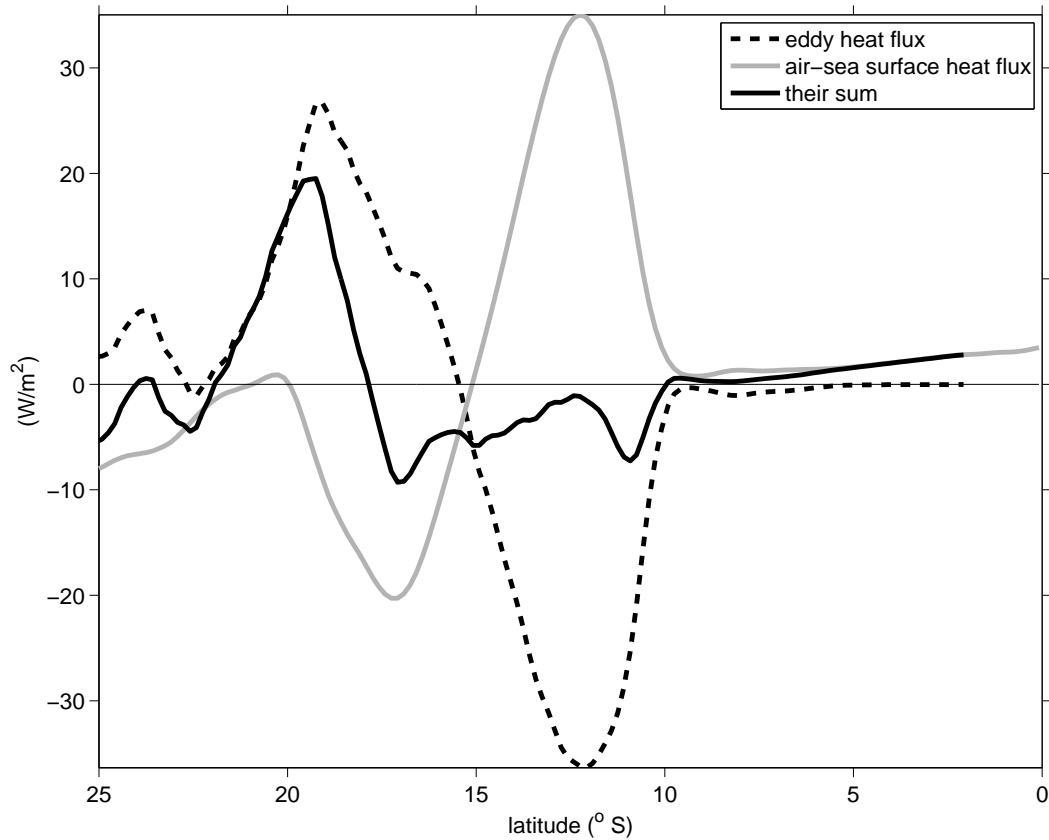


Figure 15: Zonally and time-averaged over 100 year period: divergence of the diapycnal component of eddy heat flux per unit area integrated over the mixed layer depth h , $\int_{-h}^0 \nabla \cdot [\overline{\mathbf{u}'T'} \cdot \mathbf{n}_{\mathbf{T}}] dz$, (black line), the air-sea surface heat flux H , given by Eq.(1), (grey line) and their sum (dashed line). The mixed layer depth is chosen to be 165 m, see the top panel of Fig.14. Both heat fluxes in W/m^2 . Positive flux corresponds to ocean gaining heat.

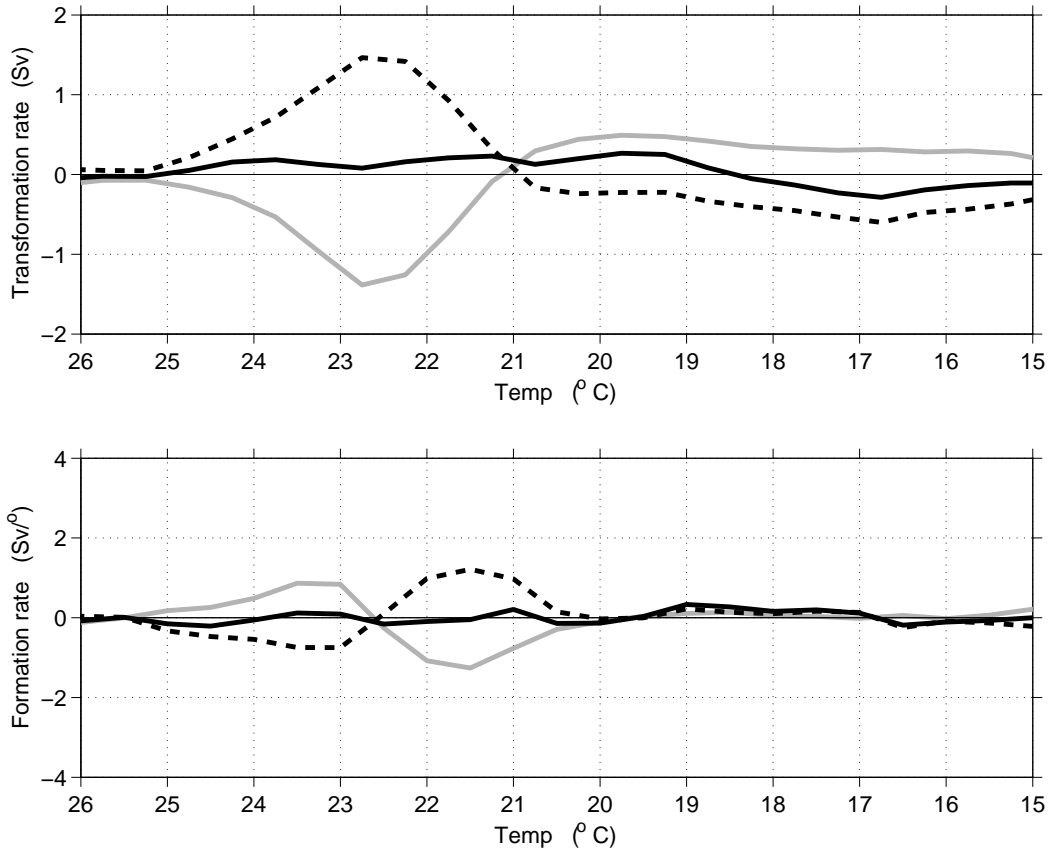


Figure 16: Top panel: volume flow across the isotherms A (in Sv) obtained from the modified Walin analysis performed on 100 years of annually averaged model temperature data. Black line shows results based on the sum of vertically integrated (over 100 m) diapycnal eddy heat flux divergence and air-sea heat flux divergence, grey line shows results from air-sea heat flux divergence and dashed line shows results from vertically integrated diapycnal eddy heat flux divergence. Bottom panel: the corresponding formation rates obtained as $\partial A/\partial T$, using the same plotting convention as in the top panel. Note the similarity between grey line and formation rate obtained from annually averaged data in Fig.12, dashed line.